Methods of Achieving Good GPR Image Resolution Using Focused SAR Processing

Mariusz Zych

Abstract—The paper describes the simulation and measurement results for a ground penetrating SAR radar. The main purpose of this paper is to present the complexity of the issues relating to GPR. Permittivity of the ground determination error causes the resolution deterioration of the resulting image therefore an important task of the digital signal processing is the correct estimation of the permittivity. The article presents several methods devoted to this subject. As a simulation model of SAR system the pulse radar with LFM (Linear Frequency Modulation) signal has been applied. The aim of the experiment is to test ability of the SAR system to obtain fully focused image of the underground targets. The real data measurements took place on the 6th floor at the Faculty of Electronics and Information – Warsaw University of Technology. During measurement campaign the GPR SAR demonstrator mounted on the rails wagon has been used to generate radar motion.

Keywords—GRP, LFM, multilook, mismatch shift.

I. Introduction

DIGITAL signal processing for GPR is much more complicated issue than in a typical radar processing. First of all typical radar deal with homogeneous medium, almost all of the radars, which analyze airspace measurements assume value of air permittivity equal to 1. GPR detects objects located underground, transmitted wave is propagated through a heterogeneous medium. The soil is composed of many layers with different permittivity coefficients. Knowledge of the permittivity of tested soil is necessary to achieve well-focused SAR image. For this reason the article is devoted to proper methods of estimating this important parameter.

In the case of the radar GPR there can be distinguished two basic methods of obtaining good azimuth resolution – coherent (focused SAR) and non-coherent (Hough transform). The majority of publications related to GPR use Hough transform for underground imaging [1] while better results are obtained using SAR [2]. In the literature there can be found few experiments of using coherent radars with SAR processing applied for underground targets imaging [3]. The main limitation of this method is greater computational complexity than in Hough transform. To create SAR image, platform with antennas in motion versus scene under observation is needed [4]–[6].

II. Geometry for Ground Penetrating Radar

The signal received by GPR comes not only from objects under interest but also from discontinuity of permittivity at

Mariusz Zych is with Radar Signal Processing Department, Przemysłowy Instytut Telekomunikacji S.A., Warsaw, Poland and The Institute of Electronic Systems, Warsaw University of Technology, Warsaw, Poland (email: zychm2@pit.edu.pl).
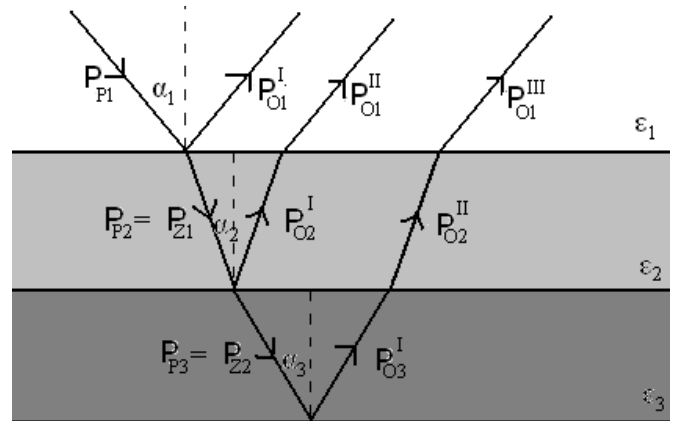
Fig. 1.   Reflection from the medium boundary.

the boundary of two different layers. The transition from one layer to another is associated with the loss of power. Moreover, an electromagnetic wave changes direction and velocity of propagation v_0 [1], [7]:

$$v_0 = \frac{1}{\sqrt{\epsilon\mu}} = \frac{1}{\sqrt{\epsilon_0\epsilon_r\mu_0\mu_r}} = \frac{c}{\sqrt{\epsilon_r\mu_r}} = \frac{c}{n}, \qquad (1)$$

where:
ϵ – permittivity,
n – refraction coefficient.

When an electromagnetic wave with power P_p falls on the border of two mediums, refraction and reflection phenomena are presented in Fig. 1.

The angle at which the reflected wave P_0 is propagated is equal to α. The rest of the transmitted power $P_z = P_p(1-\rho^2)$ passes to next medium. Concerning the relationship between the reflected P_0, transmitted P_p and refracted P_z wave powers reflection coefficients ρ [1], [7] can be used:

$$\rho = \frac{n_{(i+1)} - n_i}{n_{(i+1)} + n_i} = \frac{\sqrt{\epsilon_{r(i+1)}} - \sqrt{\epsilon_{ri}}}{\sqrt{\epsilon_{r(i+1)}} + \sqrt{\epsilon_{ri}}}, \qquad (2)$$

where:
i – number of layer.

Fig. 2 shows transmitted powers across the border of two centers as a function of permittivity. The different graphs correspond to different permittivity of first medium.

Especially we are interested in the chart corresponding to $\epsilon_r = 1$. This is the case of signal transition from the air to soil. Buried objects under GPR observation are usually characterized by different permittivity coefficient from surrounding soil. This discontinuity causes the wave reflection therefore, it is possible to detect an object, which is presented in Fig. 3.
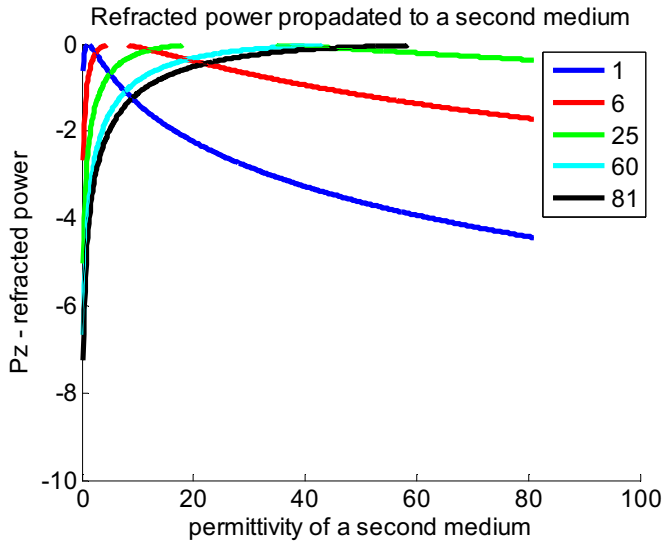
Fig. 2.   Power of refracted wave.

Fig. 4.   Radar scenario.

This chart shows the power of reflected signal as a function of permittivity.

Simulated object has permittivity $\epsilon_r = 6$. Analysis of Fig. 3. shows that even a slight difference between permittivity of the object and ground cause reflected power at level from -75 to -25 dB.

Refraction coefficients n of electromagnetic waves depend not only on the layer, but also on the wavelength. In the case of a wave with several frequency components each of them is refracted at different angle [8]:

$$n^2(\lambda) = 1 + \sum_i \frac{A_i \lambda^2}{\lambda^2 - B_i}, \tag{3}$$

where:
A_i, B_i – coefficients corresponding to the i-layer.

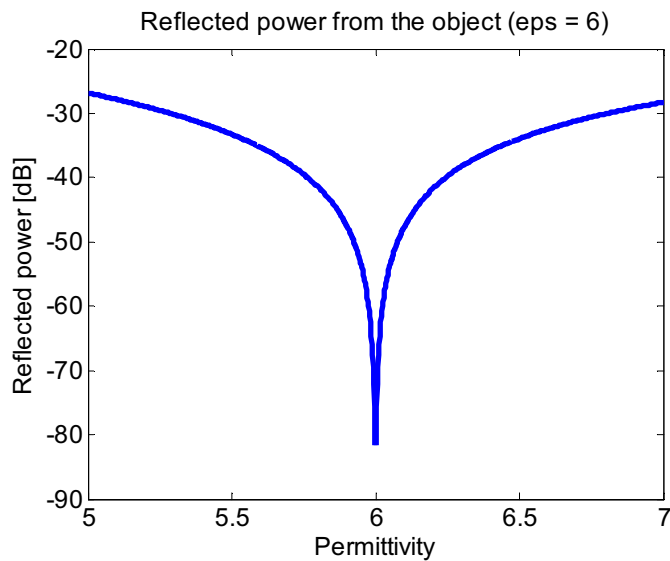Fig. 4. shows a situation where the radar is moving at a constant speed V.

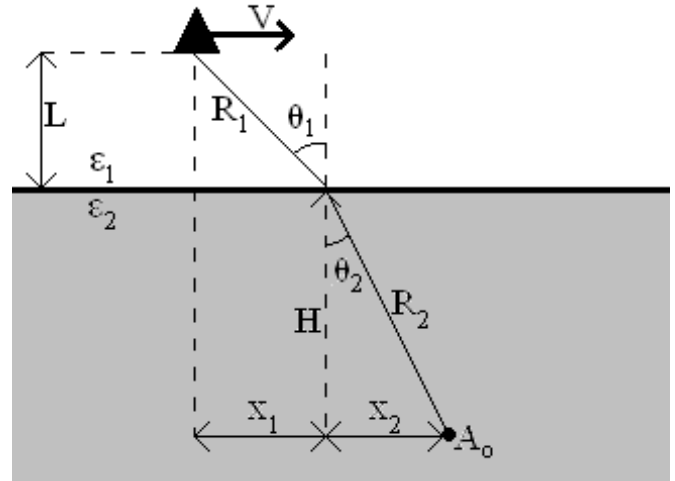Fig. 3.   Reflected power from the object as a function of ground permittivity.

This scenario was used for further simulations. The distance traveled by the wave between the transmitting antenna to the object is expressed as follows:

$$r(x) = \sqrt{L^2 + (x_1)^2} + \sqrt{H^2 + (x_2)^2}. \tag{4}$$

Presented simulations using signal with linear frequency modulation (LFM) with a pulse repetition frequency $f_{PRF} = 400$ Hz. The platform with radar moves with constant velocity $V = 2$m/s. Permittivity of the ground has been assumed for simulation as $\epsilon_r = 6$. Chirp pulse duration is equal to $\tau = 5$ns and bandwidth $B = 2$GHz which gives compression ratio of LFM pulse $C_r = B\tau = 10$.

III. SIMULATION RESULTS

Data received by GPR require digital signal processing in order to obtain acceptable resolution. Good azimuth and range resolution allows the image to be readily interpreted by operator. The image of a buried target generated by a GPR does not correspond to its geometrical representation. GPR image from one point object is similar to the curve, it is showed in Fig. 5.

The simulation which is presented above is carried out for GPR data after range compression. Six buried single points objects are present and the deepest object is barely visible. Signal received form single reflected point has the shape of a curve. Targets can be found at the following depths 0.35, 0.37, 0.4, 0.45, 0.5, 0.95 [m]. One of the best ways to improve azimuth resolution is applying focused SAR algorithm [4]–[6]. Traditional focused SAR algorithm is one-dimensional matched filtering. This article presents a method of two-dimensional SAR filtering. It uses filters matched to the depth of the object as well as the permittivity coefficient. The shape of the curve depends on these two factors. Two-dimensional convolution of compressed data S(u,v) and matched filter F(n,m) can be calculated [4], [5], [9]:

$$S_{out}(n, m) = S_0(u, v) \otimes h(n, m) =$$

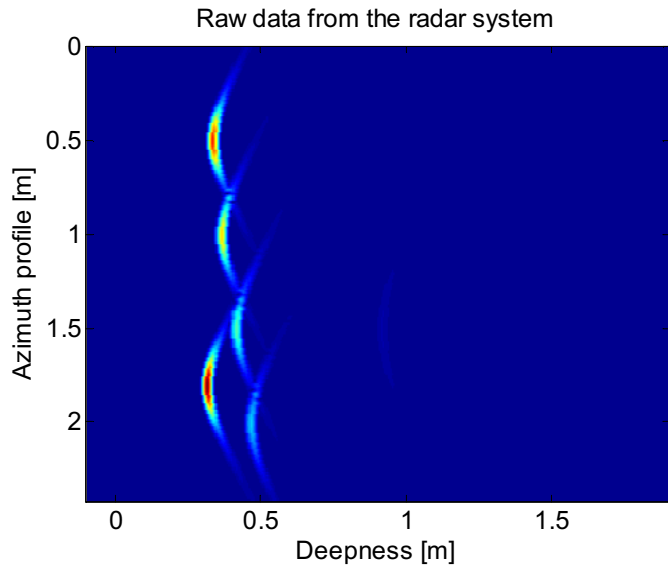$$\sum_{u=-\infty}^{\infty} \sum_{v=-\infty}^{\infty} S_0(u, v) \cdot h(n - u, m - v). \tag{5}$$

Fig. 5.   Shape of signal from single point.

Fig. 7.   Focused SAR image.

To achieve well-focused SAR image received signal is first divided into blocks according to the scheme (see Fig. 6) [2], [10].

At each step of filtering algorithm, matched filter corresponding to a given block b_i is calculated. Filter is characterized by two sizes – permittivity of the medium and depth of the object. These two factors have an influence on the shape of the curve of filter. Filtered block is then multiplied by Hamming window:

$$w(n) = 0.5 - 0.5 \cdot \cos\left(\frac{2\pi n}{3 \cdot N_{BL}}\right), \qquad (6)$$

where: $n = 0, 1, 2, \ldots - 1$.

The appearance of focused SAR image after applying filtration for raw data presented in Fig.5. is visible in Fig. 7.

Simulations show that the correlation of raw data after range compression with the filter gives the desired resolution in the different variants of dielectric permittivity coefficient and depth of the object. For this reason, permittivity need to be provisionally estimated for tested soil.

The target showed in Fig. 8 is buried at a depth of three meters, permittivity coefficient of the layer is 4 (at the middle of the chart). The chart shows the maximum value of focused image after SAR processing for one point object as a function of permittivity and the depth. For different values of permittivity of the soil and the depth of the object similar results
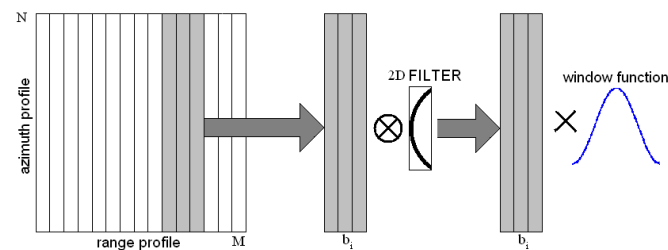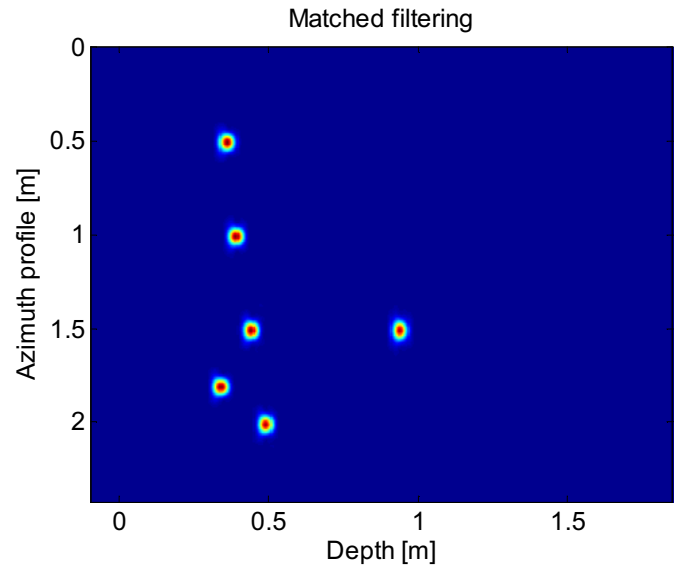
has been obtained. According to what has been showed it is difficult to determine these parameters.

A common method for correct estimation of the desired parameters is an algorithm of optimizing image contrast. Incorrectly chosen value of permittivity cause blurring of the final image, therefore it is possibility of finding correct permittivity based on obtained contrast. Objective is to optimize the contrast given by formula:

$$C = \frac{E\{[I^2(x,y) - E[I^2(x,y)]]^2\}}{E[I^2(x,y)]}, \qquad (7)$$

where:
E – expected value
$I(x,y)$ – value of the pixel.

The effectiveness of the algorithm has been tested for six single point objects shown in Fig. 5. Real value of permittivity
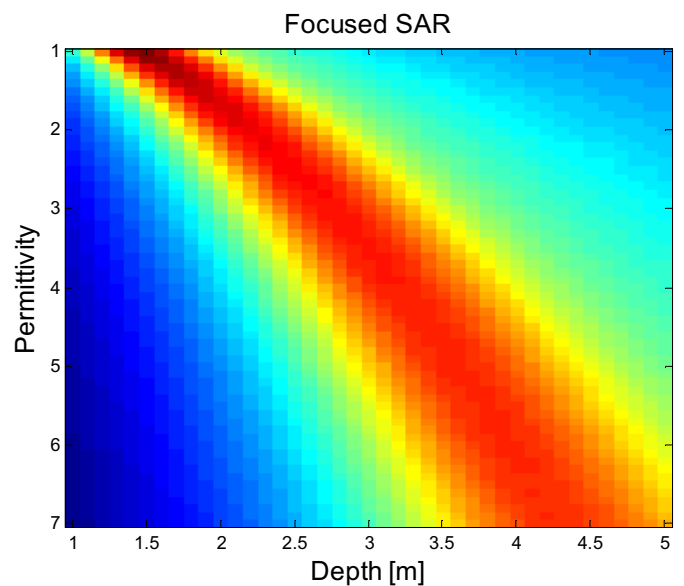
Fig. 6.   2D SAR filtration.

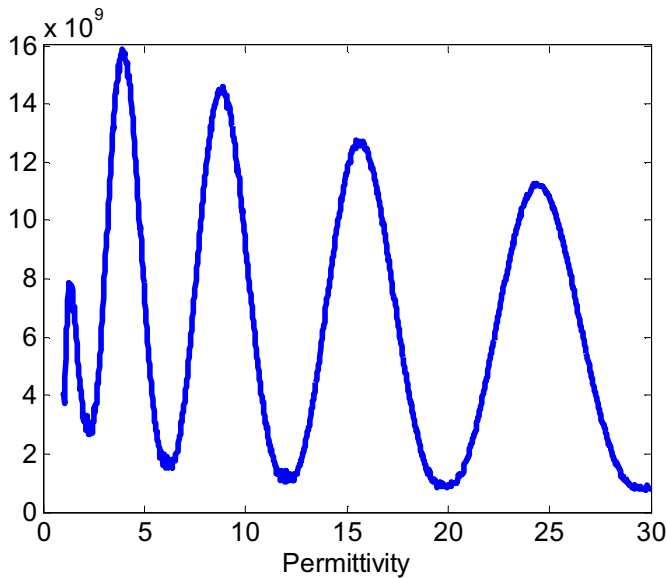Fig. 8.   Ambiguity of parameters.

Fig. 9.   The results of contrast optimizing.

Fig. 11.   Ambiguity of object parameters.

is $\epsilon_r = 9$.

The results of two-dimensional SAR filtering are not satis-factory. The image does not determine the correct permittivity, what is more it points wrong value of this parameter. The function has a sinusoidal shape, one of its peaks pointing to the correct permittivity but this is not appropriate solution of estimating correct value of permittivity.

To determine focused SAR parameters the multilook algo-rithm has been applied. Multilook algorithm assumes division of the main beam of the antenna [9], [10]. Matched filtration is carried out for each of the received sub-beams. Images are then deposited in a coherent way. The concept of multilook algorithm is presented in Fig. 10.

Having shifted images, it is possible to get well focused image on the condition of well-matched filters and well-defined velocity of the radar. When the filters are mismatched shift dx between focused images from each beam is obtained. After combining the information about amplitude of focused image and achieved shift from multilook method, the following result has been obtained (Fig. 11).

To correctly specify parameters of matched filter there is a need to estimate initial value of permittivity. Knowledge of one of the parameters allows to designate the second of them. The appearance of shift function dx for object buried at a depth of 3 m, for ground permittivity 4 is showed at Fig. 12. The function passes through the value 0 for the correct permittivity value, at a constant depth. In fact, mere knowledge of the
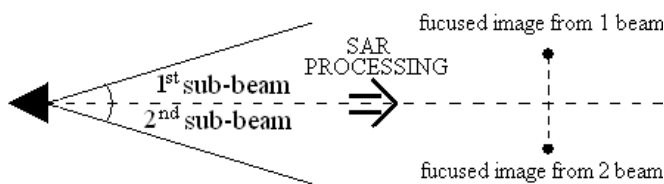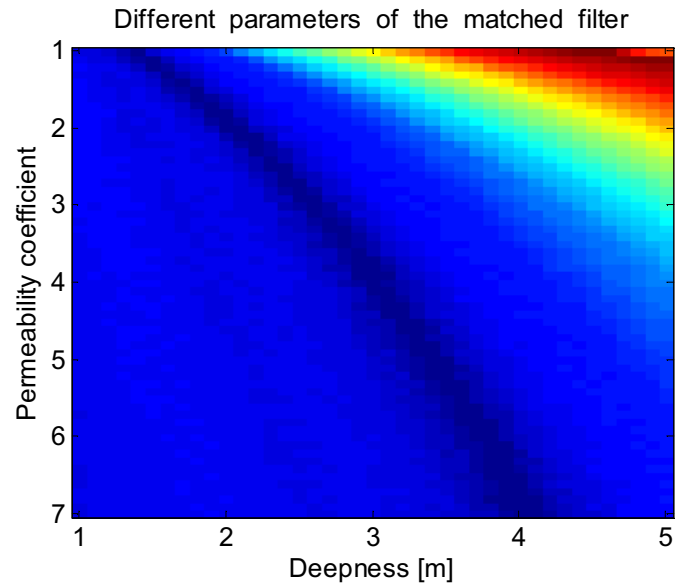
permittivity of the analyzed soil determine the depth of the object.

In the same way we can investigate the dx parameter depen-dence of range at a constant value of permittivity coefficient.

Considering received echo from six single points object shown in Fig. 7 it is possible to achieve real value of soil permittivity. Maximum value of cross-correlation for each range cell is determined. Index of this maximum in the azimuth direction for every range cell is given by formula:

$$\kappa(m) = \max\left\{\sum_{n=0}^{N-1} Y^1(n,m) \cdot Y^{2^*}(n-k,m)\right\}, \quad (8)$$

where:
n – index of cells in azimuth direction,
m – index of cells in range direction,
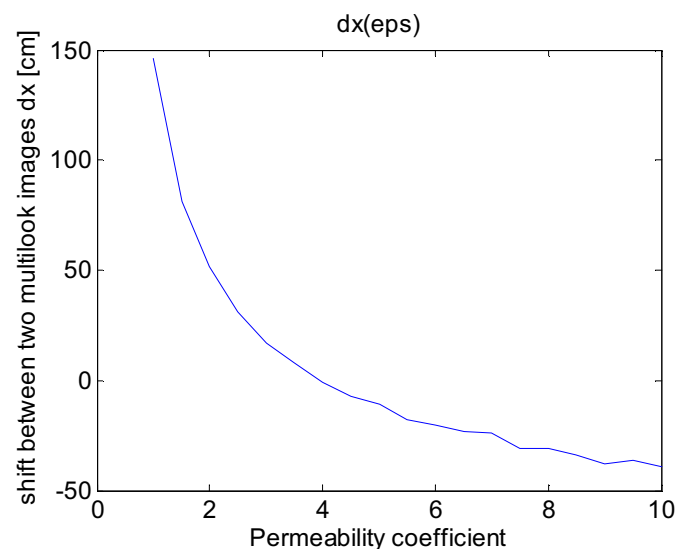$Y^i(n,m)$ – value of the pixel for i-multilook image.

Fig. 10.   Multilook concept.

Fig. 12.   Epsilon influence on matched filtering.

Fig. 13.   Depth influence on matched filtering.
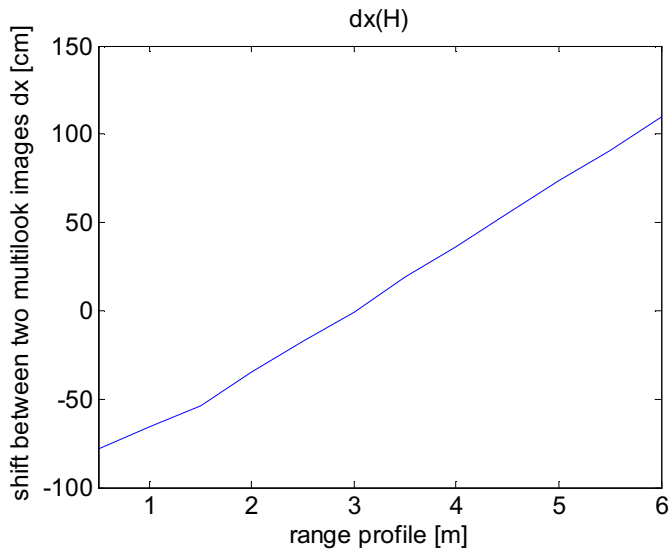

Fig. 15.   Noise generator.

Main beam of the antenna has been divided into two parts, parameters of mismatched shift dx are summed for every range cell [2]:

$$\rho_x = \sum_{m=0]}^{M-1} (\kappa(m) - N). \qquad (9)$$

Analysis of parameter ρ_x as a function of permittivity is shown in Fig. 14. The function reaches a minimum value for the correct permittivity which is equal to 6 for this experiment.

IV. MEASUREMENT RESULTS

Real measurement has been made using noise signal generated by serially connected wideband amplifiers (0.8 – 2.4 GHz). Each amplifier has a gain equal to 20 dB. Measurement system is shown in Fig. 15.

Measurement has been made on the 6th floor at the Faculty of Electronics and Information – Warsaw University of
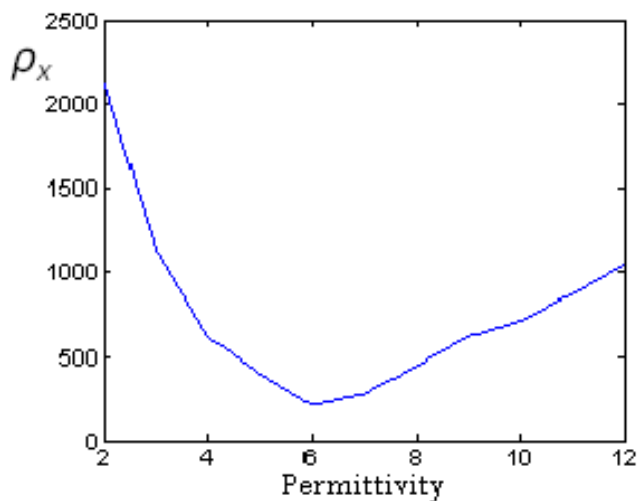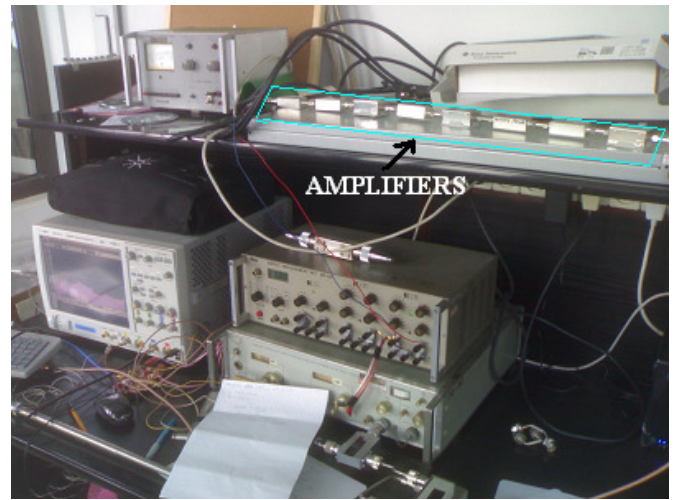
Technology using rail wagon controlled by computer. Spacing between antennas is L = 0.64m, antennas were located at the height of 0.5m above the balcony. Main purpose of the measurement is to achieve cross-sectional image of the faculty. In order to eliminate direct crosstalk adaptive lattice filter has been applied. Measurement results after range compression is shown in Fig. 17.

The final image after focused SAR algorithm is shown in Fig. 18. Reflections from each of the targets can be easily seen.

V. CONCLUSIONS

- Simulation results for GPR imaging presented in the paper show that it is possible to use SAR processing for underground targets imaging.
- Obtained results require further investigation. An iterative method of permittivity estimation is planned in future.
- Presented ground penetrating radar could be used to investigate the soil structure, unless the permittivity coefficients is correctly determined.
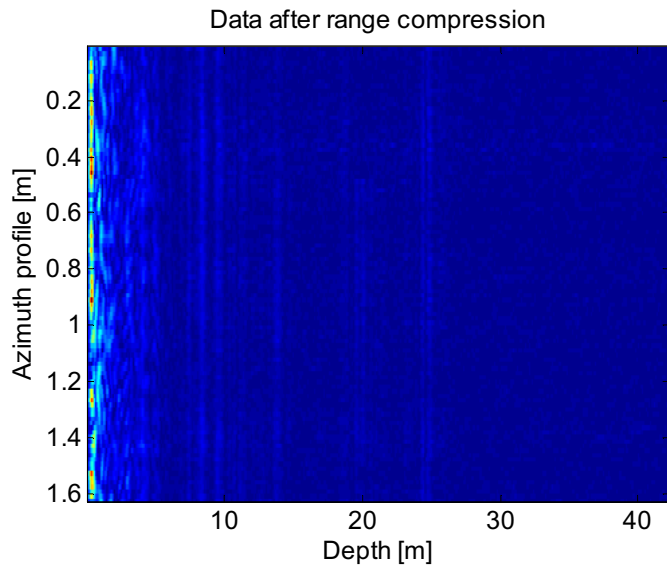

Fig. 14.   Estimation of permittivity.

Fig. 16.   Antennas used in measurement.

Data after range compression

Fig. 17.   Data after range compression.

Image after SAR processing

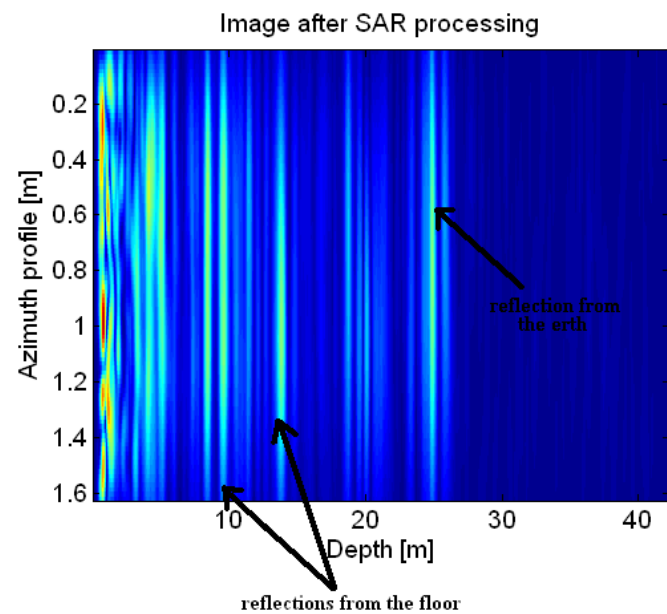Fig. 18.   Image after focused SAR algorithm.

REFERENCES

[1] D. J. Daniels, *Ground Penetrating Radar, 2nd edition*, The Institution of Engineering and Technology, London, 2007.
[2] M. Zych, "Comparison of Using SAR Processing and Hough Transform as Methods for GPR Rdar Image Creation," in *Radar Methods and Systems Workshop*, Kiev, Ukraine, 21-23 September 2010.
[3] I. Nicolaescu and P. van Genderen, "Procedures to Improve the Performances Used for Landmine Detection," in *Microwaves, Radar and Remote Sensing Symposium*, Kiev, Ukraine, September 22-24 2008.
[4] J. C. Curlander and R. N. McDonough, *Synthetic Aperture Radar, Systems and Signal Processing*.   Canada: John Wiley & Sons Inc., 1991.
[5] W. G. Carrara, R. S. Goodman, and R. M. Majewski, *Spotligth Synthetic Aperture Radar – Signal Processing Algorithms*.   London: Artech House Inc., 1995.
[6] I. G. Cumming and F. H. Wong, *Digital Processing of Synthetic Aperture Radar Data*.   London: Artech House Inc., 2002.
[7] M. I. Skolnik, *Introduction to Radar Systems*, 2nd ed.   McGraw-Hill, Inc., 1981.
[8] S. Khedim, A. Chiali, and B. Benyoucef, "Calculation of Refractive Index of Some Materials," in *Revue des Energies Renouvelables ICRESD-07*, Tlemcen, 2007.
[9] M. Zych, D. Gromek, and A. Gromek, "Focused Algorithms for Ground Penetrating Radar Imaging," in *International Radar Symposium*, Vilnius, Lithuania, 2010.
[10] M. Zych, "Focused Methods of Digital Signal Processing for Ground Penetrating Radar – GPR," in *1st Conference of Students research group at The Faculty of Electronics and Information Technology*.   Warsaw, Poland: Warsaw University of Technology, 12 October 2010.